Schottky Barrier Formation and Strain at the (011) GdN/GaN Interface from First Principles

Toshiya Kagawa
Department of Physics, Yokohama National University, Yokohama, Japan

Hannes Raebiger*
Department of Physics, Yokohama National University, Yokohama, Japan and Centro de Ciências Naturais e Humanas, Universidade Federal do ABC, Santo André, São Paulo, Brazil

(Received 11 August 2014; revised manuscript received 24 October 2014; published 14 November 2014)

GdN and GaN are both insulators, the former being also a ferromagnet. Despite a lattice mismatch of 10.1% and different crystal structures, lattice-matched interfaces where GdN adopts the smaller lattice parameter of GaN can be formed. We study isotropically and epitaxially strained GdN, as well as the nonpolar (011) GdN/GaN interface by first-principles calculation. We show that upon compressive strain (isotropic or biaxial) corresponding to the strain imposed by the GaN lattice, GdN becomes a half-metallic ferromagnet. In the interface calculation, however, no magnetization of GaN at or away from the interface is observed. The interface exhibits a Schottky connection with the GdN Fermi energy 1.19 eV above the GaN valence band (close to midgap); i.e., the system can be used as a rectifier and possibly also for spintronic applications.

DOI: 10.1103/PhysRevApplied.2.054009

I. INTRODUCTION

Rare-earth pnictides (*R*-V) in rocksalt structure are often metallic and offer a lattice-matched contact to tetrahedral III-V semiconductors. In particular, ErAs/GaAs and ErAs/InGaAs are widely studied as a prototype system for various applications ranging from thermoelectric power generators [1,2] to gigahertz-to-terahertz sources and detectors [3–5]. The GdN/GaN interface [6] emerges as the wide band gap and transparent alternative to ErAs/GaAs systems, with the additional prospect of spintronics applications due to the ferromagnetism of GdN. Despite the recent success of GdN nanoisland-based GaN tunnel junctions [7], the physical properties of the underlying GdN/GaN interface remain poorly known. To this end, we investigate the GdN/GaN interface by first-principles calculation.

GdN is an indirect-gap insulator with a rocksalt structure and a ferromagnet with a Curie temperature of $T_C \sim 60$ K [8–14]. The lattice mismatch between GdN and GaN is approximately 10%, GdN being larger than GaN. Nonetheless, lattice-matched epitaxial films and nanoislands have been successfully grown on GaN substrates [6,7,15,16] or even MgO substrates with an even larger lattice mismatch of approximately 19% [17]. Combining these observations with the fact that GaN is harder than GdN suggests that thin films or nanoislands of GdN adopt the GaN lattice parameter and are heavily strained. This diversifies the physics of the GdN/GaN interface, because on the one hand, interface strain is likely to affect the band lineup, and on the other hand, the electronic and magnetic properties of GdN are reportedly very sensitive to strain [18,19].

We first show that GdN becomes a half-metallic ferromagnet upon biaxial (or hydrostatic) strain such as imposed by the GaN substrate. In principle, this can be the ideal interface for spin injection [20–22]. We investigate this system by direct calculation of the nonpolar (011) interface of rocksalt GdN and zinc-blende GaN. Band profiles along the interface normal show that while GdN maintains its half-metallic properties, there is little to no magnetization of GaN, which, thus, also maintains its nonmagnetic properties. We further evaluate the band lineup of this interface, which we find to be a Schottky-type contact with the GdN Fermi level inside the GaN band gap at 1.19 eV above the GaN valence-band top. This confirms that the GdN/GaN interface, indeed, is very similar to ErAs/GaAs [23] and offers a wide band-gap transparent alternative to ErAs/GaAs systems with the additional feature that GdN is a ferromagnet at low temperatures. Moreover, the GdN/GaN interface as such is already a rectifier, which means it could offer an alternative to applications based on *p*-*n* junctions. GdN may also become useful as a spin injector into GaN, or ferromagnetic Mn-, Fe-, or Gd-doped GaN (see, e.g., Refs. [24–31]).

II. DETAILS OF CALCULATION

In order to describe structural and electronic properties of the GdN/GaN interface, first-principles total-energy calculations within the projector augmented-wave (PAW) method [32] are carried out using the VASP code [33,34].

*hannes@ynu.ac.jp

Plane waves are included up to the cutoff energy of 350 eV. The exchange correlation energy is approximated by the Perdew-Burke-Enzerhof (PBE) generalized gradient approximation (GGA) functional, where, however, including $+U$ corrections on Gd d and f electrons is crucial to reproduce the correct band structure of GdN [13,35–37]. We use the potential parameters $U_d = 3.4$, $J_d = 0$, $U_f = 8.0$, and $J_f = 1.2$ (in eV) given by Larson and Lambrecht [35]. The Ga d electrons, on the other hand, are treated as core electrons, i.e., not explicitly included in the PAW potential. Inclusion of the Ga d electrons with appropriate $+U$ correction leads to the shrinking of the GaN lattice parameter by approximately 5% [38], which will exaggerate the interface strain in slab calculations. We consider GaN in the zinc-blende structure to construct a nonpolar slab model for the interface described below.

A. Interface model

To study an interface, we consider a slab model consisting of N layers of GdN followed by N layers of GaN, repeated periodically, called an "N/N slab" henceforth. We limit this study to the [011] direction, which is nonpolar for both rocksalt and zinc-blende structures; a slab constructed in a polar direction contains two different interfaces whose interface properties cannot unambiguously be deconvoluted, and one also may encounter artificially created electric fields by charge densities accumulated at the interface [39,40]. Because GaN is harder and practical applications are likely to involve nanoislands or thin films of GdN deposited on bulk GaN, we assume GdN to adopt the lateral lattice constant of GaN a_{in}; this assumption seems reasonable for nanoislands of only a few nanometers in size, covered by GaN on both sides as described in Refs. [7,16] but may fail for thin films as the film thickness increases beyond some threshold value. The slab width L is relaxed, as are all nuclear coordinates inside the slab supercell. A schematic illustration of a 7/7 slab is given in Fig. 1. Convergence tests for the slab width are described together with the calculation results. Brillouin-zone sampling is done by a Monkhorst-Pack $13 \times 9 \times 1$ $\vec{k}$ mesh.

B. Band alignment

GdN under biaxial strain due to the GaN substrate becomes a metal, and to characterize the semiconductor-metal interface, we calculate the band alignment or band offset at this interface. In the Schottky-Mott limit, the band alignment of two materials is simply the difference between the metal work function and semiconductor band edge. Local-density functionals, like the PBE GGA used in the present work, notoriously underestimate the band gap, mostly attributed to a too-low-lying conduction band, so we focus on the alignment of the valence-band edge ε_{VBM} and metal work function (Fermi level) E_F. We calculate the (p-type) Schottky barrier height ϕ_p as [41,42]

$$\phi_p = E_F - \varepsilon_{\text{VBM}} - \Delta\bar{\bar{V}}. \quad (1)$$

Here, $\Delta\bar{\bar{V}}$ is the change in average electrostatic potential across the interface (positive, if higher on the semiconductor side), calculated using the macroscopic averaging method [43–45]. E_F and ε_{VBM} are given referenced to the average electrostatic potentials of the respective (strained) bulk materials. For a Schottky-type connection, $0 < \phi_p < E_g$ (E_g is the semiconductor band gap); otherwise, the connection is Ohmic.

III. BULK MATERIALS

GaN is a direct-gap semiconductor that exists in both wurtzite and zinc-blende phases, wurtzite being the ground-state structure. Both structures are wide-gap semiconductors with similar properties; the zinc-blende phase has a

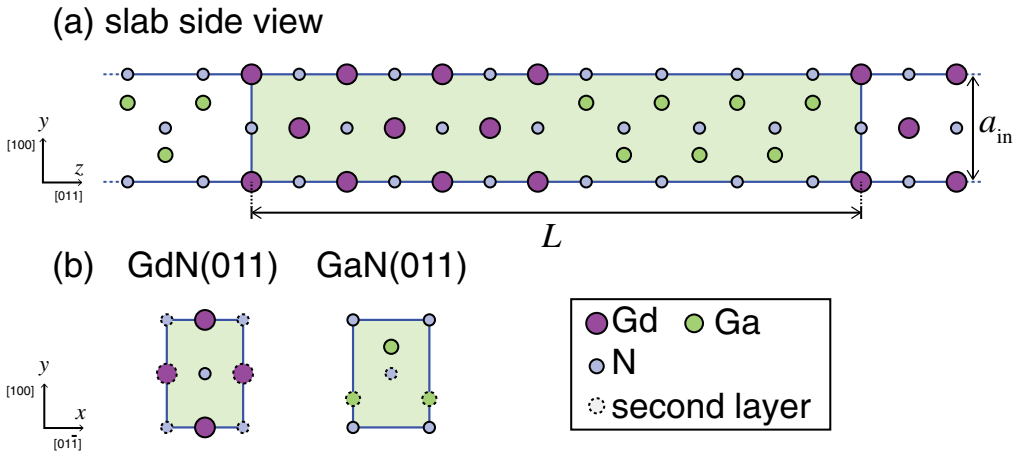

FIG. 1. (a) Schematic representation of the slab of the 7/7 model of the rocksalt-zinc-blende (011) interface and (b) the (011) layers of the rocksalt and zinc-blende structures. The shaded region of (a) indicates the slab unit cell. L and a_{in} are the slab width and the in-plane lattice parameter, respectively.

TABLE I. Lattice parameter a, elastic constants C_{11}, C_{12}, and C_{44}, and the bulk modulus B calculated for (zinc-blende) GaN and GdN.

	GaN	GdN
a	4.59 Å	5.11 Å
B	180 GPa	138 GPa
C_{11}	255 GPa	274 GPa
C_{12}	143 GPa	69.5 GPa
C_{44}	173 GPa	108 GPa

slightly smaller band gap of approximately 3.3 eV than the wurtzite-phase band gap of approximately 3.4 eV. Our calculation gives a gravely underestimated band gap of 1.47 eV due to the well-known local-density approximation (LDA) error. The lattice constant of $a = 4.59$ Å as well as elastic constants as shown in Table I are well in agreement with available experimental and calculated values (see, e.g., Refs. [46–49] and references therein).

GdN is a ferromagnetic indirect-band-gap semiconductor. We find an equilibrium lattice parameter of $a = 5.11$ Å; the (unstrained) band structure calculated at this equilibrium is given in Fig. 2. Initially, there was much controversy of whether GdN is a semimetal with small band overlap (half-metallic ferromagnet), a zero-gap semiconductor, or a finite-gap semiconductor. Much of this controversy is caused by the band-gap error of local-density approximations, which erroneously predicts a half-metallic band structure. Experimentally, GdN is a semiconductor [12,13], and correcting the band-gap error by onsite $+U$ corrections on Gd d and f electrons [13,35–37] predicts a ferromagnetic semiconducting band structure as shown in Fig. 2. The valence-band top is at Γ, and the conduction-band bottom at X. The bands are spin polarized, so majority (+) and minority (−) spin components have different gaps $E^{\Gamma\text{-}X}_{\text{gap}+} = 0.28$ eV (0.12 eV) and $E^{\Gamma\text{-}X}_{\text{gap}-} = 1.06$ eV (1.25 eV); the direct X-X gaps are $E^{X}_{\text{gap}+} = 0.66$ eV (0.57 eV) and $E^{X}_{\text{gap}-} = 1.29$ eV (1.39 eV)—the values given in parentheses are those calculated by Larson and Lambrecht [35], well in agreement with the present work.

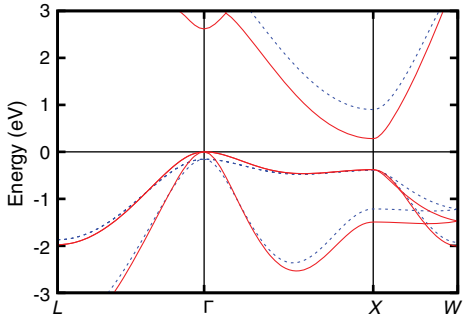

FIG. 2. GdN band diagram. The solid (red) and dashed (blue) lines denote majority and minority spin components, respectively. The valence-band top is set as zero energy.

The elastic constants and bulk modulus calculated for GdN are given in Table I. These agree well with those given by Mankad *et al.* [50] despite the fact that their ground-state structures are metallic due to the band-gap error in their local-density functional. This confirms that the elastic properties of GdN are not that sensitive to band-gap errors or even to the qualitatively different electronic structures (metal vs insulator). GdN does not exhibit transitions from low to high spin states or other dramatic changes in electron structure that will require special corrections, such as, e.g., position- or strain-dependent $+U$ corrections [51–53]. We follow by investigating how the band structure of GdN evolves under hydrostatic and epitaxial strain.

Figure 3 shows that upon small hydrostatic compression ($-8\% < \delta < -4\%$) GdN becomes a semimetal with zero band gap. Upon compression, the valence bands are shifted to higher energies. The shift is not rigid; i.e., the conduction-band bottom at X is lowered with respect to the valence-band top, and at the same time, the valence-band shoulder at X is shifted upwards in energy, closing up the direct gap $E^{X}_{\text{gap}+}$, until at a compression of approximately 8% or more, the X gap closes up [Fig. 3(b)]. Notice that the gap is closed up only for the majority spin component; i.e., the band structure is half-metallic. Hydrostatic expansion, on the other hand, opens up E^{X}_{gap}, but a conduction-band local minimum at Γ approaches the valence-band top, as seen in Fig. 3(c). These trends in band structure due to

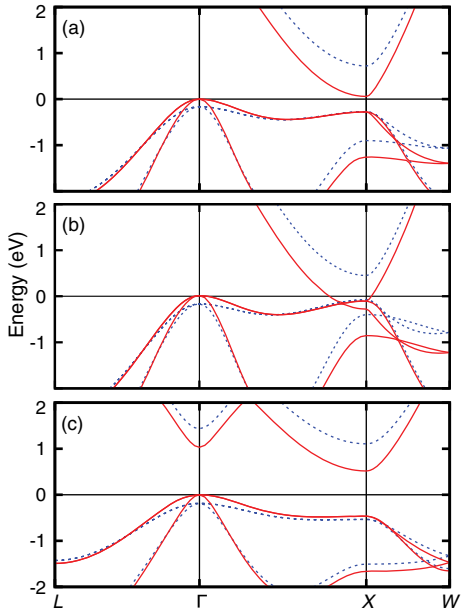

FIG. 3. GdN band structure under hydrostatic strain of (a) $\delta = -4\%$, (b) $\delta = -8\%$, and (c) $\delta = +8\%$. The solid (red) and dashed (blue) lines denote majority and minority spin components, respectively. The highest-occupied electronic state (valence-band top for semiconductor, Fermi energy for metal) is set as zero energy.

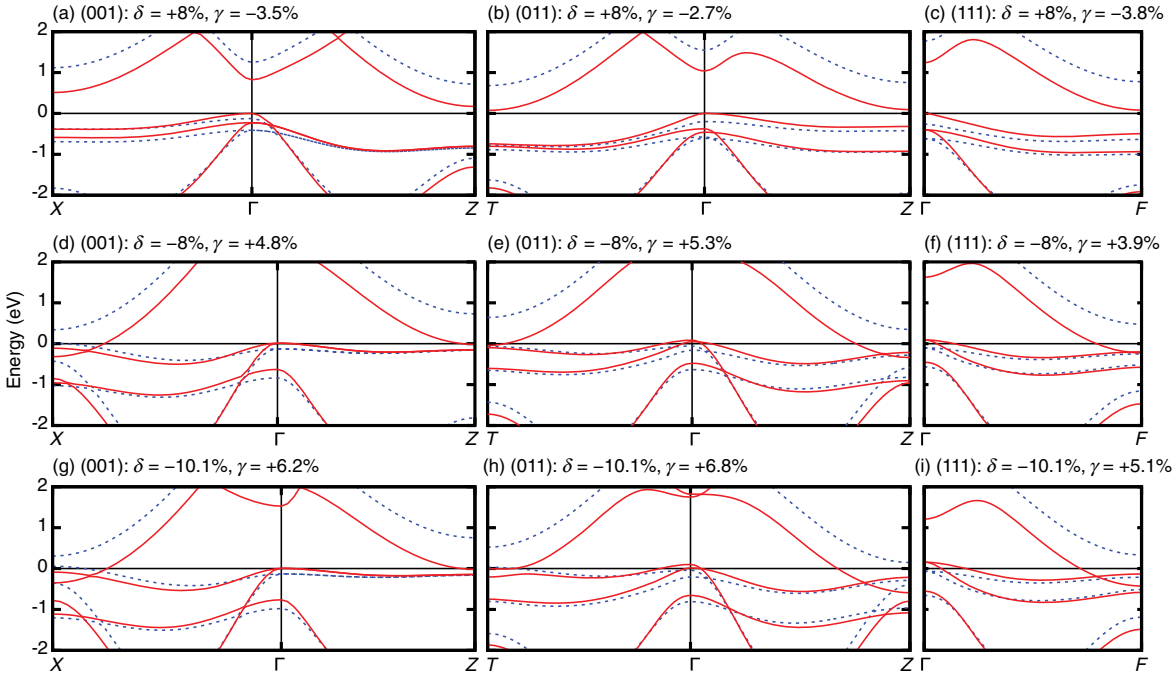

FIG. 4. GdN band structure under biaxial strain. Tensile and compressive stress of of $\delta = +8\%$, -8%, and -10.1% in (001), (011), and (111) orientations with perpendicular distortion γ as indicated in panels (a)–(i). Legend and energy scale as in Fig. 3.

hydrostatic strain are qualitatively similar as shown by Duan *et al.* [18], albeit the conclusions are strikingly different. Duan *et al.* predicted a metallic ground state for GdN (due to the LDA error) and show that hydrostatic expansion opens up the gap to form a half-metal, semimetal, or semiconductor. Our ground state is semiconducting, and we show that compression closes up the gap, making GdN a half-metal. The upshot is that such compression can be achieved by epitaxially growing GdN on a substrate with a smaller lattice constant, albeit that gives biaxial strain rather than isotropic strain.

We consider biaxial strain for the (001), (011), and (111) orientations. We fix the in-plane lattice parameter to a value strained by δ, with positive and negative δ meaning tensile and compressive strains, respectively. When strain is applied biaxially, a perpendicular relaxation also takes place: tensile (compressive) strain of $(\pm)\delta$ yields compression (expansion) of $(\mp)\gamma$ in the perpendicular direction. The relation γ/δ is well described by $\frac{\gamma}{\delta} = \frac{2\nu}{1-\nu}$ with the relatively small Poisson ratio of $\nu \approx 0.2$ (in agreement with Duan *et al.* [18]).

The biaxially strained band structures for the (001), (011), and (111) orientations are given in Fig. 4. The effects are essentially the same as described above for the isotropic strain: tensile strain opens up the gap, whereas compressive strain closes the gap and turns GdN into a half-metal. However, due to the strain, the symmetry of the Brillouin zone has changed, which may lead to different (anisotropic) conductive properties than in the isotropically strained system. Upon biaxial strain in the (001), (011), and (111) directions, the unit cell becomes body-centered tetragonal, body-centered orthorhombic, and rhombohedral, respectively. For (001) strain, we have four equivalent X and two Z points corresponding to the six equivalent X points of the unstrained system; here, only the E^X_{gap} closes up, leaving a small direct band gap E^Z_{gap}, which may limit conductivity perpendicular to the interface. For (011) strain, both E^T_{gap} (fourfold symmetry) and E^Z_{gap} (twofold symmetry) close up individually, and for (111) strain, the closing of E^F_{gap} (sixfold symmetry) is as discussed above for the isotropic strain. Interestingly, the valence-band spin splitting for GdN biaxially compressed in the (001) and (011) directions seems to be inverted at the fourfold X and T points, respectively. Nonetheless, there is still a gap for minority spin bands at these points, and even at $\delta = -10.1\%$, we expect half-metal behavior. However, larger compression is likely to induce a transition from half-metallic to a metallic (ferromagnetic) phase.

IV. GdN/GaN (011) INTERFACE

The lattice mismatch between GdN and zinc-blende GaN for our optimized structures is $\delta = -10.1\%$. Compressing the GdN biaxially to match the GaN lattice gives an expansion of $\gamma = 6.8\%$ in the perpendicular direction, which yields a separation of 1.93 Å between the GdN (011) layers. The separation between the GaN (011) layers is 1.62 Å. We carry out calculations for 7/7, 9/9, and 11/11 interface slabs, and find that the layer separations in both GdN and GaN regions farthest away from the interface correspond to the biaxially strained bulk values within ± 0.01 Å; i.e., all slabs considered are sufficiently large to

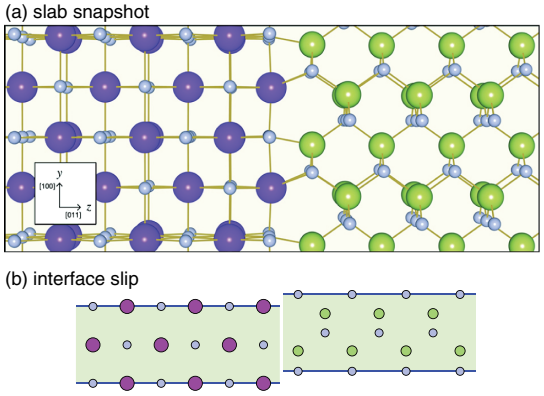

FIG. 5. (a) Snapshot of relaxed GdN/GaN interface. (b) Schematic illustration of slipping parallel to the interface; cf. "ideal interface" in Fig. 1(a). Purple, green, and gray spheres represent Gd, Ga, and N atoms, respectively.

reproduce bulk strain properties far away from the interface. Unless otherwise stated, the results and data presented henceforth are calculated for the 9/9 slab.

Both zinc-blende and rocksalt structures are based on fcc sublattices for both anions and cations. Thus, in principle, the nitrogen sublattice can be perfectly continuous across the interface. However, as seen in Fig. 5, the lattice planes are slipped parallel to the interface by about 15% of the GaN lattice constant (approximately 0.7 Å), which is larger than the 10% slipping at the GaAs/ErAs (011) interface [23]. We follow by evaluating real-space band structures and band lineups.

To visualize the real-space band structure across the interface, we evaluate the real-space density of states $\rho(z;E)$ projected onto the normal direction z of the interface [54–61]. This projection is calculated for majority and minority spins $\sigma = \pm$ as

$$\rho_\sigma(z;E) = \int\int_S dxdy \sum_i |\psi_{i\sigma}(\vec{r})|^2 \delta(E-\varepsilon_{i\sigma}). \quad (2)$$

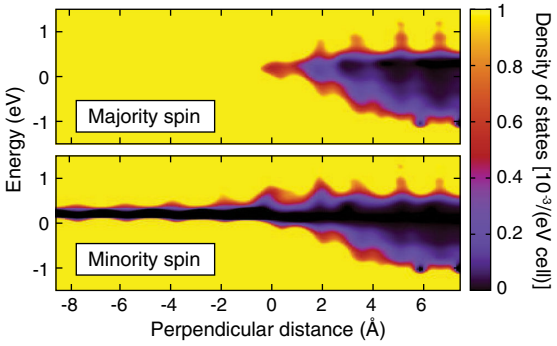

FIG. 6. Band profile perpendicular to the (011) GdN/GaN interface. Fermi energy is set as zero energy. The interface is at 0 Å; GdN and GaN layers are on the negative and positive sides, respectively. Density-of-states values $\rho(z;E) > 10^{-3}$ states/(eV cell) are truncated (yellow area).

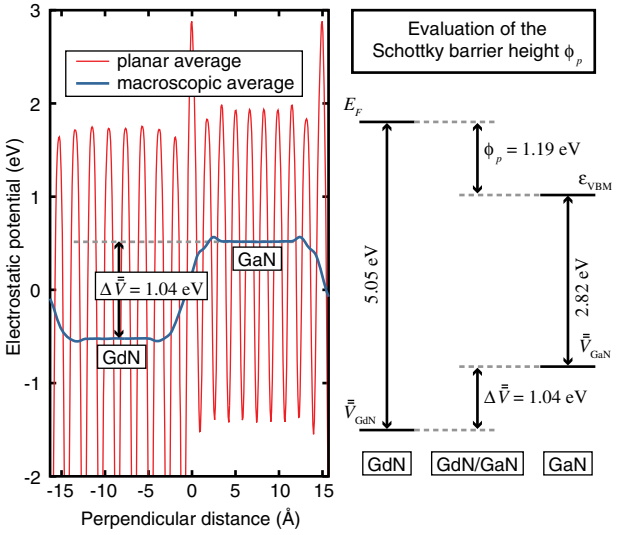

FIG. 7. Electrostatic potential and Schottky barrier evaluation. The planar electrostatic potential (red line) exhibits lattice plane oscillations, which are filtered out by macroscopic averaging (blue line). The GdN E_F and GaN ε_{VBM} are evaluated with respect to the average electrostatic potentials of (strained) GdN $\bar{\bar{V}}_{GdN}$ and (unstrained) GaN $\bar{\bar{V}}_{GaN}$, respectively.

Here, $\psi_{i\sigma}$ and $\varepsilon_{i\sigma}$ are Kohn-Sham orbitals and eigenvalues, respectively, and S is the cross section of the slab supercell. $\rho_+(z;E)$ and $\rho_-(z;E)$ shown in Fig. 6 show that for majority spin, the band gap closes immediately at the interface, whereas the minority spin bands maintain a band gap; i.e., GdN recovers its bulk properties almost immediately (first ML) away from the interface. GaN recovers its bulk band structure more smoothly, but at four to five ML (>6 Å) away from the interface, GaN recovers its GGA band gap. Despite the strong spin polarization (half-metallic behavior) of GdN, there is no noticeable spin polarization of GaN. Thus, both materials maintain their bulklike magnetizations. The Fermi energy (set as zero in Fig. 6) is inside the GaN band gap, so based on the band profile, the interface exhibits a Schottky connection. Notice that Fig. 6 shows the spatial region where electronic states exist $[\rho(z;E) \neq 0]$ but not necessarily gives an accurate estimate of Schottky barrier heights. Far away from the interface, $\rho(z;E)$ does converge to the bulk density of states, but its convergence is much slower than that of the charge density, and using $\rho(z;E)$ to estimate Schottky barrier heights will require larger slabs and a larger $\vec{k}$ mesh for Brillouin-zone sampling [56].

We calculate the Schottky barrier height of $\phi_p = 1.19$ eV using Eq. (1), as shown in Fig. 7, where E_F and ε_{VBM} are evaluated from the strained ($\delta = -10.1\%$) and unstrained bulk calculations of GdN and GaN, respectively. The above ϕ_p is calculated for the 9/9 slab, and for final confirmation of slab convergence, we evaluate $\phi_p = 1.23$ eV and $\phi_p = 1.20$ eV for the 7/7 and 11/11 slabs, respectively. Spin-orbit coupling effects neglected

here lead to an uncertainty in this numerical value, but we expect the effect to be in the order of approximately 0.1 eV here [62]; many-body corrections may lead to a further uncertainty (of similar magnitude) to the GaN valence-band edge, as the GGA band-gap error is mostly due to a too-low-lying conduction band (see, e.g., Refs. [30,38,63]). Thus, we may safely conclude that the GdN E_F is in the middle of the GaN band gap, and the n-type Schottky barrier can be evaluated as $\phi_n = E_{\mathrm{gap}} - \phi_p \approx 2.1$ eV using the experimental value for the GaN band gap.

The GdN Fermi level with respect to $\bar{\bar{V}}_{\mathrm{GdN}}$ is 5.09 and 5.07 eV for systems strained in the (001) and (111) directions with $\delta = -10.1\%$ corresponding to the GaN host, i.e., nearly the same as for the (011) strained value of 5.05 eV. Thus, any significant difference to $\phi_p = 1.19$ for different orientations can be due only to the band lineup $\Delta\bar{\bar{V}}$. The bonding and polarity and interface relaxations differ for the different interface orientations, and $\Delta\bar{\bar{V}}$ is not likely to be constant. For the ErAs/GaAs system, the Schottky barrier differs by approximately 0.2 eV for (001)- and (011)-oriented interfaces [23], which may indicate the order of magnitude of differences $\Delta\bar{\bar{V}}$ in the different orientations. Thus, we may safely assume that also the (001)- and (111)-oriented interfaces are Schottky connections.

V. CONCLUSION

We present a first-principles calculation of the (011) GdN/GaN interface together with a study of GdN under isotropic and epitaxial strain. We first show that unstrained GdN is a ferromagnetic indirect band-gap insulator, which under compressive strain exhibits a transition to a half-metal state. This transition occurs under both isotropic and biaxial compressive strain in (001), (011), or (111) directions, and the threshold strain for this transition lies in the range $\delta = -4\%, \ldots, -8\%$ for isotropic strain; biaxially strained GdN with strain greater than $\delta = -8\%$ is a half-metal regardless of strain direction. In particular, GdN biaxially strained by $\delta = -10.1\%$ exhibits half-metal properties, which corresponds to the lattice strain of nanoislands or thin films of GdN deposited on GaN substrates.

We carry out detailed calculations of the (011) GdN/GaN interface, which we find to exhibit a Schottky connection with the GdN Fermi level (work function) 1.19 eV above the GaN valence band, i.e., Schottky barrier of $\phi_p = 1.19$ eV. Assuming that differences in band lineup for other interface orientations are not larger than this Schottky barrier, also the (001) and (111) interfaces will be Schottky connections, albeit with a slightly different Schottky barrier. Despite the half-metallic ferromagnetism of GdN, spin polarization of GaN at and away from the interface is negligible. GdN recovers its (strained) bulk properties already in the first or second layer next to the interface, and GaN becomes bulklike at four to five ML (>6 Å) away from the interface. The interface inherently behaves as a rectifier and may also be useful for spintronics applications.

ACKNOWLEDGMENTS

H. R. thanks the São Paulo Research Foundation (FAPESP) for financial support.

[1] J. M. Zide, D. O. Klenov, S. Stemmer, A. C. Gossard, G. Zeng, J. E. Bowers, D. Vashaee, and A. Shakouri, Thermoelectric power factor in semiconductors with buried epitaxial semimetallic nanoparticles, Appl. Phys. Lett. **87**, 112102 (2005).

[2] G. Zeng, J. E. Bowers, J. M. O. Zide, A. C. Gossard, W. Kim, S. Singer, A. Majumdar, R. Singh, Z. Bian, Y. Zhang, and A. Shakouri, ErAs:InGaAs/InGaAlAs superlattice thin-film power generator array, Appl. Phys. Lett. **88**, 113502 (2006).

[3] M. Griebel, J. H. Smet, D. C. Driscoll, J. Kuhl, C. Alvarez Diez, N. Freytag, C. Kadow, A. C. Gossard, and K. von Klitzing, Tunable subpicosecond optoelectronic transduction in superlattices of self-assembled ErAs nanoislands, Nat. Mater. **2**, 122 (2003).

[4] A. C. Young, J. D. Zimmerman, E. R. Brown, and A. C. Gossard, Semimetal-semiconductor rectifiers for sensitive room-temperature microwave detectors, Appl. Phys. Lett. **87**, 163506 (2005).

[5] J. F. O'Hara, J. M. O. Zide, A. C. Gossard, A. J. Taylor, and R. D. Averitt, Enhanced terahertz detection via ErAs:GaAs nanoisland superlattices, Appl. Phys. Lett. **88**, 251119 (2006).

[6] M. A. Scarpulla, C. S. Gallinat, S. Mack, J. S. Speck, and A. C. Gossard, GdN (111) heteroepitaxy on GaN (0001) by N_2 plasma and NH_3 molecular beam epitaxy, J. Cryst. Growth **311**, 1239 (2009).

[7] S. Krishnamoorthy, T. F. Kent, J. Yang, P. S. Park, R. C. Myers, and S. Rajan, GdN nanoisland-based GaN tunnel junctions, Nano Lett. **13**, 2570 (2013).

[8] D. B. McWhan, Effect of pressure on the Curie temperature and volume of GdN, J. Chem. Phys. **44**, 3528 (1966).

[9] R. J. Gambino, T. R. McGuire, H. A. Alperin, and S. J. Pickart, Magnetic properties and structure of GdN and $GdN_{1-x}O_x$, J. Appl. Phys. **41**, 933 (1970).

[10] P. Wachter and E. Kaldis, Magnetic interaction and carrier concentration in GdN and $GdN_{1-x}O_x$, Solid State Commun. **34**, 241 (1980).

[11] D. X. Li, Y. Haga, H. Shida, T. Suzuki, Y. S. Kwon, and G. Kido, Magnetic properties of stoichiometric Gd monopnictides, J. Phys. Condens. Matter **9**, 10777 (1997).

[12] S. Granville, B. J. Ruck, F. Budde, A. Koo, D. Pringle, F. Kuchler, A. Preston, D. Housden, N. Lund, A. Bittar, G. V. M. Williams, and H. J. Trodahl, Semiconducting ground state of GdN thin films, Phys. Rev. B **73**, 235335 (2006).

[13] H. J. Trodahl, A. R. H. Preston, J. Zhong, B. J. Ruck, N. M. Strickland, C. Mitra, and W. R. L. Lambrecht, Ferromagnetic redshift of the optical gap in GdN, Phys. Rev. B **76**, 085211 (2007).

[14] K. Senapati, T. Fix, M. E. Vickers, M. G. Blamire, and Z. H. Barber, Structural evolution and competing magnetic orders in polycrystalline GdN films, Phys. Rev. B **83**, 014403 (2011).

[15] F. Natali, B. Ludbrook, J. Galipaud, N. Plank, S. Granville, A. Preston, B. L. Do, J. Richter, I. Farrell, R. Reeves, S. Durbin, J. Trodahl, and B. Ruck, Epitaxial growth and properties of GdN, EuN and SmN thin films, Phys. Status Solidi (c) **9**, 605 (2012).

[16] T. F. Kent, J. Yang, L. Yang, M. J. Mills, and R. C. Myers, Epitaxial ferromagnetic nanoislands of cubic GdN in hexagonal GaN, Appl. Phys. Lett. **100**, 152111 (2012).

[17] J. W. Gerlach, J. Mennig, and B. Rauschenbach, Epitaxial gadolinium nitride thin films, Appl. Phys. Lett. **90**, 061919 (2007).

[18] C.-G. Duan, R. F. Sabiryanov, J. Liu, W. N. Mei, P. A. Dowben, and J. R. Hardy, Strain induced half-metal to semiconductor transition in GdN, Phys. Rev. Lett. **94**, 237201 (2005).

[19] H. Yoshitomi, R. Vidyasagar, S. Kitayama, T. Kita, H. Ohta, S. Okubo, Y. Fukuoka, and T. Sakurai, Ferromagnetic properties of GdN thin films studied by temperature dependent circular polarized spectroscopy, Appl. Phys. Lett. **101**, 072403 (2012).

[20] S. Datta and B. Das, Electronic analog of the electro-optic modulator, Appl. Phys. Lett. **56**, 665 (1990).

[21] G. A. Prinz, Magnetoelectronics, Science **282**, 1660 (1998).

[22] S. A. Wolf, D. D. Awschalom, R. A. Buhrman, J. M. Daughton, S. von Molnar, M. L. Roukes, A. Yu. Chtchelkanova, and D. M. Treger, Spintronics: A spin-based electronics vision for the future, Science **294**, 1488 (2001).

[23] K. T. Delaney, N. A. Spaldin, and C. G. Van de Walle, Theoretical study of Schottky-barrier formation at epitaxial rare-earth-metal/semiconductor interfaces, Phys. Rev. B **81**, 165312 (2010).

[24] T. Dietl, H. Ohno, F. Matsukura, J. Cibert, and D. Ferrand, Zener model description of ferromagnetism in zinc-blende magnetic semiconductors, Science **287**, 1019 (2000).

[25] S. Dhar, O. Brandt, A. Trampert, K. J. Friedland, Y. J. Sun, and K. H. Ploog, Observation of spin-glass behavior in homogeneous (Ga,Mn)N layers grown by reactive molecular-beam epitaxy, Phys. Rev. B **67**, 165205 (2003).

[26] S. Dhar, O. Brandt, M. Ramsteiner, V. F. Sapega, and K. H. Ploog, Colossal magnetic moment of Gd in GaN, Phys. Rev. Lett. **94**, 037205 (2005).

[27] G. M. Dalpian and S.-H. Wei, Electron-induced stabilization of ferromagnetism in $Ga_{1-x}Gd_xN$, Phys. Rev. B **72**, 115201 (2005).

[28] T. Hynninen, H. Raebiger, and J. von Boehm, Structural and magnetic properties of (Ga,Mn)N from first principles, Phys. Rev. B **75**, 125208 (2007).

[29] Y. Gohda and A. Oshiyama, Intrinsic ferromagnetism due to cation vacancies in Gd-doped GaN: First-principles calculations, Phys. Rev. B **78**, 161201 (2008).

[30] A. Zunger, S. Lany, and H. Raebiger, The quest for dilute ferromagnetism in semiconductors: Guides and misguides by theory, Physics **3**, 53 (2010).

[31] T. Dietl and H. Ohno, Dilute ferromagnetic semiconductors: Physics and spintronic structures, Rev. Mod. Phys. **86**, 187 (2014).

[32] P. E. Blöchl, Projector augmented-wave method, Phys. Rev. B **50**, 17953 (1994).

[33] G. Kresse and D. Joubert, From ultrasoft pseudopotentials to the projector augmented-wave method, Phys. Rev. B **59**, 1758 (1999).

[34] G. Kresse and J. Furthmüller, Efficient iterative schemes for *ab initio* total-energy calculations using a plane-wave basis set, Phys. Rev. B **54**, 11169 (1996).

[35] P. Larson and W. R. L. Lambrecht, Electronic structure of Gd pnictides calculated within the LSDA + U approach, Phys. Rev. B **74**, 085108 (2006).

[36] P. Larson, W. R. L. Lambrecht, A. Chantis, and M. van Schilfgaarde, Electronic structure of rare-earth nitrides using the LSDA + U approach: Importance of allowing 4f orbitals to break the cubic crystal symmetry, Phys. Rev. B **75**, 045114 (2007).

[37] C. Mitra and W. R. L. Lambrecht, Magnetic exchange interactions in the gadolinium pnictides from first principles, Phys. Rev. B **78**, 134421 (2008).

[38] R. Cherian, P. Mahadevan, and C. Persson, Role of semi core levels in determining the band-gaps of semiconductors: First-principles calculations with model Hamiltonians, Solid State Commun. **149**, 1810 (2009).

[39] W. A. Harrison, E. A. Kraut, J. R. Waldrop, and R. W. Grant, Polar heterojunction interfaces, Phys. Rev. B **18**, 4402 (1978).

[40] J. Junquera, M. H. Cohen, and K. M. Rabe, Nanoscale smoothing and the analysis of interfacial charge and dipolar densities, J. Phys. Condens. Matter **19**, 213203 (2007).

[41] C. G. Van de Walle and R. M. Martin, Theoretical calculations of heterojunction discontinuities in the Si/Ge system, Phys. Rev. B **34**, 5621 (1986).

[42] S.-H. Wei and A. Zunger, Role of d orbitals in valence-band offsets of common-anion semiconductors, Phys. Rev. Lett. **59**, 144 (1987).

[43] A. Baldereschi, S. Baroni, and R. Resta, Band offsets in lattice-matched heterojunctions: A model and first-principles calculations for GaAs/AlAs, Phys. Rev. Lett. **61**, 734 (1988).

[44] L. Colombo, R. Resta, and S. Baroni, Valence-band offsets at strained Si/Ge interfaces, Phys. Rev. B **44**, 5572 (1991).

[45] M. Peressi, N. Binggeli, and A. Baldereschi, Band engineering at interfaces: Theory and numerical experiments, J. Phys. D **31**, 1273 (1998).

[46] K. Kim, W. R. L. Lambrecht, and B. Segall, Electronic structure of GaN with strain and phonon distortions, Phys. Rev. B **50**, 1502 (1994).

[47] K. Kim, W. R. L. Lambrecht, and B. Segall, Elastic constants and related properties of tetrahedrally bonded BN, AlN, GaN, and InN, Phys. Rev. B **53**, 16310 (1996).

[48] A. F. Wright, Elastic properties of zinc-blende and wurtzite AlN, GaN, and InN, J. Appl. Phys. **82**, 2833 (1997).

[49] Y. Oussaifi, A. Ben Fredj, M. Debbichi, N. Bouarissa, and M. Said, Elastic properties and optical phonon frequencies of zinc-blende $Sc_xGa_{1-x}N$, Semicond. Sci. Technol. **22**, 641 (2007).

[50] V. Mankad, S. K. Gupta, and P. K. Jha, Ab initio investigation on structural, electronic and lattice dynamical properties of MgN and GdN crystals, Results Phys. **2**, 34 (2012).

[51] T. Tsuchiya, R. M. Wentzcovitch, C. R. S. da Silva, and S. de Gironcoli, Spin transition in magnesiowüstite in Earth's lower mantle, Phys. Rev. Lett. **96**, 198501 (2006).

[52] H. Hsu, K. Umemoto, M. Cococcioni, and R. Wentzcovitch, First-principles study for low-spin $LaCoO_3$ with a structurally consistent Hubbard U, Phys. Rev. B **79**, 125124 (2009).

[53] H. J. Kulik and N. Marzari, Accurate potential energy surfaces with a DFT + U(R) approach, J. Chem. Phys. **135**, 194105 (2011).

[54] C. Berthod, N. Binggeli, and A. Baldereschi, Local interface dipoles and the tuning of the Al/GaAs(100) Schottky-barrier height with ultrathin Si interlayers, Europhys. Lett. **36**, 67 (1996).

[55] C. Berthod, N. Binggeli, and A. Baldereschi, Formation energy, lattice relaxation, and electronic structure of Al/Si/GaAs(100) junctions, Phys. Rev. B **57**, 9757 (1998).

[56] M. Peressi, N. Binggeli, and A. Baldereschi, Band engineering at interfaces: Theory and numerical experiments, J. Phys. D **31**, 1273 (1998).

[57] Y. Yamashita, S. Yamamoto, K. Mukai, J. Yoshinobu, Y. Harada, T. Tokushima, T. Takeuchi, Y. Takata, S. Shin, K. Akagi, and S. Tsuneyuki, Direct observation of site-specific valence electronic structure at the SiO_2/Si interface, Phys. Rev. B **73**, 045336 (2006).

[58] F. Devynck, Ž. Šljivančanin, and A. Pasquarello, Electronic properties of an epitaxial silicon oxynitride layer on a 6H-SiC(0001) surface: A first-principles investigation, Appl. Phys. Lett. **91**, 061930 (2007).

[59] T. Shirasawa, K. Hayashi, H. Yoshida, S. Mizuno, S. Tanaka, T. Muro, Y. Tamenori, Y. Harada, T. Tokushima, Y. Horikawa, E. Kobayashi, T. Kinoshita, S. Shin, T. Takahashi, Y. Ando, K. Akagi, S. Tsuneyuki, and H. Tochihara, Atomic-layer-resolved bandgap structure of an ultrathin oxynitride-silicon film epitaxially grown on 6H-SiC(0001), Phys. Rev. B **79**, 241301 (2009).

[60] Y. Ando, Y. Gohda, and S. Tsuneyuki, Dependence of the Schottky barrier on the work function at metal/SiON/SiC(0001) interfaces identified by first-principles calculations, Surf. Sci. **606**, 1501 (2012).

[61] B. Zhang, W. Lin, S. Li, Y. Zheng, X. Yang, D. Cai, and J. Kang, Ohmic contact to n-AlGaN through bonding state transition at TiAl interface, J. Appl. Phys. **111**, 113710 (2012).

[62] S. Picozzi, A. Continenza, G. Satta, S. Massidda, and A. J. Freeman, Metal-induced gap states and Schottky barrier heights at nonreactive GaN/noble-metal interfaces, Phys. Rev. B **61**, 16736 (2000).

[63] S. Lany, H. Raebiger, and A. Zunger, Magnetic interactions of Cr-Cr and Co-Co impurity pairs in ZnO within a band-gap corrected density functional approach, Phys. Rev. B **77**, 241201 (2008).